ISBN: 978-3-95450-208-0 doi:10.18429/JACoW-IPAC2019-THPTS024

MAGNET DEVELOPMENTS AND PRECISE ALIGNMENT SCHEMES FOR SPRING-8-II

K. Fukami*[1], T. Aoki. N. Azumi[1], H. Kimura[1], S. Takano[1], T. Taniuchi, S. Matsubara,
K. Yanagida, T. Watanabe[1], C. Zhang, JASRI, 679-5198 Hyogo, Japan
S. Matsui, RIKEN SPring-8 Center, 679-5148 Hyogo, Japan
S. Inoue, T. Kai, J. Kiuchi, SPring-8 Service Co., Ltd., 679-5165 Hyogo, Japan
[1]also at RIKEN SPring-8 Center, 679-5148 Hyogo, Japan

Abstract

The magnet lattice design of the SPring-8 upgrade, SPring-8-II, is a five bend achromat composed of one normal and four longitudinal gradient bending magnets. Permanent magnet has been chosen for both types of the dipoles, and the high gradient multipole magnets are all electromagnets. We have designed and fabricated test magnets and developed precise alignment schemes. In 2018, we constructed a test half-cell with the test magnets by applying our alignment procedures. This presentation will overview the magnet developments and precise alignment schemes for SPring-8-II, including the result of the test half-cell construction.

INTRODUCTION

The new optics of the storage ring for upgraded SPring-8, SPring-8-II, based on a five-bend achromat lattice has been designed and the corresponding key components have been developed. The new lattice is expected to provide the natural emittance of about 150 pmrad without any extra radiation damping [1]. Each cell has 5 bending magnets, 20 quadrupole magnets, and 10 sextupole magnets. For obtaining adequate dynamic aperture in the low emittance ring, the alignment tolerance of the magnets in the transverse plane is much smaller than for the present ring. The series of multipole magnets on a straight section between bending magnets, which are placed on a common girder, must be aligned with a standard deviation of 25 μm or less. The common girders must be aligned each other with a standard deviation of 45 μm or less. These require alignment tolerances are ±50 μm and ±90 μm, respectively.

Prototype bending magnets, multipole magnets and common girders for the half cell lattice were fabricated to test these performances and to check a physical interference with other instruments, and to demonstrate the alignment on the common girder. We present our alignment scheme, and discuss the error budget on the scheme in this paper.

MAGNET DEVELOPMENTS

One of feature of the magnet system is a permanent based bending magnet for substantial energy saving. Layout of magnets in a half cell lattice is shown in Fig. 1. Quadrupole and sextupole magnets are named from *Q01* to *Q10*, and *SD1*, *SF1* etc. in each cell, and the magnets with the same name are excited in series by one power supply. Common girders on the straight sections are named *A*, *B* and *C* from the upstream end of the cell.

Permanent-Magnet-Based Bending Magnets

For SPring-8-II, what we call longitudinal gradient bends are planned to be installed so that electrons are to be bent in a large angle when dispersion is small, and are bent in a small angle when dispersion is large. In our case, a single bending magnet is split into three segments with different dipole fields for generating a three-step field distribution [2]. These years several facilities have discussed a possibility of permanent magnets for their future accelerators, and we have also worked on it especially paying attention to the reliability, stability, and usability of such magnets [3]. So far, we have fabricated normal bending magnets, longitudinal gradient bending magnets, and a septum magnet based on permanent magnet. The magnets are equipped with the magnetic field adjustability based on our outer/inner plate mechanisms, a magnetic circuit that compensates the temperature dependence of permanent magnet material [3]. We have chosen Sm_2Co_{17} material that is known to have a high radiation-resistance. In 2018, one of the normal bending magnets was installed in the beam transport between the booster synchrotron and the storage ring of SPring-8, and has been dedicated to user operation for a year. The one-year experience with the permanent dipole magnet shows that no notable drift or deteriorations related to the permanent magnet has been observed.

Electromagnet-Based Multipole Magnets

Major parameters of the multipole magnets are listed in Table 1. Cores are made of 0.5-mm thick laminated steel. All the magnets are water-cooled type. We set the current density of hollow conductors to less than 3.4 A/mm^2 to suppress the power loss and the deformation of the magnets. To prevent interference between coil ends of magnets and other instruments, magnetic poles are tapered in the longitudinal direction. Some sextupole magnets have auxiliary coils to add steering functions.

A good field region is here defined as the region in which the field gradient homogeneity is within 0.1 %. To maintain the good field region of ±8 mm for quadrupole magnets and ±6 mm for sextupole magnets both in horizontal and vertical directions, a shape of the shimming was optimized at the pole edge. We set an individual difference among one family, which are excited by common power supply, to less

* fukami@spring8.or.jp

ISBN: 978-3-95450-208-0 doi:10.18429/JACoW-IPAC2019-THPTS024

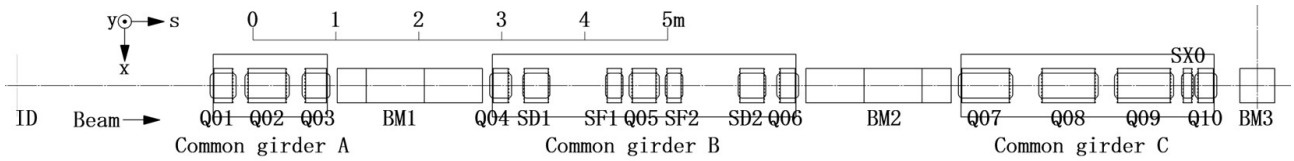

Figure 1: Layout of magnets in a half cell lattice. Length is 14.952 m. The symbols *BM** indicate permanent based bending magnets. Two of these, *BM1* and *BM2*, are longitudinal gradient bends (see text in detail). The symbols *Q** and *S** indicate quadrupole magnets and sextupole magnets, respectively. Remaining half cell lattice is arranged symmetrically with the longitudinal center line of *BM3* as a symmetrical axis. Coordinate axes and positive directions are also shown.

than 0.1 %. The field profiles and the individual differences will be measured using a stretched wire system [4].

To install the vacuum chamber, top halves of cores of the magnets are reassembled after the precise alignment. The change in the magnetic center caused by the reassembly increases the total alignment error. To suppress the change, we adopted a conventional keyway structure at the joint of the cores. For the magnets of *Q04*, *Q05* and *SD1*, we directly measured the changes using the vibrating-wire alignment technique described later. We repeated five times the reassembly and measurement. The peak-to-peak value of the changes was less than ±3 µm.

Table 1: Major Parameters of the Multipole Magnets

Parameter	Quadrupole	Sextupole
Bore diameter	34 mm	36 mm
Maximum gradient	56 T/m	2730 T/m^2
Effective length	200-700 mm	112-300 mm
Maximum current	352 A	250 A
Turn number	20 T/Pole	9 T/Pole

Common Girders for Multipole Magnets

Four-point support was adopted to suppress a deformation caused by a vertical variation of the floor, and to simplify adjustment process [5]. We have designed a load deflection to less than 50 µm, and an eigenfrequency to larger than 110 Hz. We fabricated the prototype common girders *A*, *B* and *C* by different welding methods and height adjustment mechanism to test a rigidity and performance for the alignment. We confirmed that the load deflection was suppressed by an inexpensive welding, e.g., a fillet welding.

PRECISE ALIGNMENT SCHEME

A vibrating-wire alignment technique has commonly been used for such high-precision alignments [6]- [8]. A tensioned wire, excited with an AC current, is placed along the longitudinal axis in a series of magnets. The field profile of a multipole magnet near its magnetic center can be measured by detecting the vibration of the wire at its resonance frequency. We have adopted this method to align the series of multipole magnets on the common girders, taking advantage of the feature that one can align the magnets while directly observing the magnetic center of each magnet without fiducialization.

After the alignment on the common girder is carried out at an external experiment room, the common girders and multipole magnets are transported to the accelerator tunnel. At the tunnel, the common girders and bending magnets are aligned using a laser tracker system.

Vibrating-Wire Alignment Technique

Two wire girders made of Super-Inver were placed at both ends of each of the common girders *B* and *C* [9]. We stretched a 4.1-m-long Be-Cu wire 0.2 mm in diameter with a tension of 2 kgf. We chose a heat-treated wire, NGK Ltd., C1720W-EHM, based on the observation of the sag profile shown below. We set a frequency of driving current to the fundamental-resonance, and measured the wire vibration in the *x*-*y* plane using a laser sensor (KEYENCE Ltd., LS-9000D). A vibration amplitude and a phase at the driving frequency were detected using a lock-in amplifier. The wire ends were placed on *x*-*y* stages with a resolution of 0.1 µm. We excited magnets separately, and then, found the magnetic centers by scanning the wire using the *x*-*y* stages. For each common girder, we defined the straight line passing through the magnetic centers of both end magnets as the reference line. We measured displacement between the reference line and magnetic centers of the other magnets.

The sag profile in longitudinal direction of a tensioned wire is given by a catenary curve [6]. The maximum sag S_{max} at the center of the wire is expressed as

$$S_{max} = \frac{\rho}{8T} L^2 = \frac{g}{32 f_1^2}, \quad (1)$$

where T [kgf] is the tension and ρ [kgf/m] is the wire density, L [m] is the wire length, f_1 [Hz] is the fundamental-resonance frequency and g [m/sec^2] is the acceleration due to gravity. The nominal maximum sag is 0.28 mm, and is not negligible. In conventional vibrating-wire techniques, the maximum sag is determined from the measured frequency. It is assumed that the sag profile follows the theoretical curve [6]. However, sag profile of actual wire does not exactly follow the theoretical curve, owing to local kink and other reason. In this study, to choose a suitable wire, we investigated the sag full profile of actual wires using a sag observation bench. We stretched the Be-Cu wire above a movable stage at the tension of 2 kgf. We placed one sensor of the wire-positioning system (FOGALE Ltd., WPS) on the movable stage and used it to measure the height distribution of the wire along the longitudinal direction. The center of the wire in the longi-

ISBN: 978-3-95450-208-0 doi:10.18429/JACoW-IPAC2019-THPTS024

tudinal direction is defined to be s=0. We moved the stage along s-axis over the range of ±2 m in step of 10 mm.

We fitted the measured sag to the catenary curve, and defined a residual sag error as the difference between the measured sag and the fitted value. Example of the residual sag error along s-axis is shown in Fig. 2. We observed local kinks in 4 wires in 10 individual test wires. The maximum amplitude was 5 µm, and the maximum width was 30 mm. The local kinks induce a random error, however, the kinks are averaged over the length of the magnet. The moving average over 0.3 m, which is the typical length of test magnet, is also shown in Fig. 2. The average value was as small as the surrounding region. In contrast, periodic residual sag error was observed for an no heat-treated wire with an amplitude of 4 µm and a period of 250 mm [9]. It is assumed that such wire deteriorates the total random error because the periodic error is not drastically suppressed by the moving average.

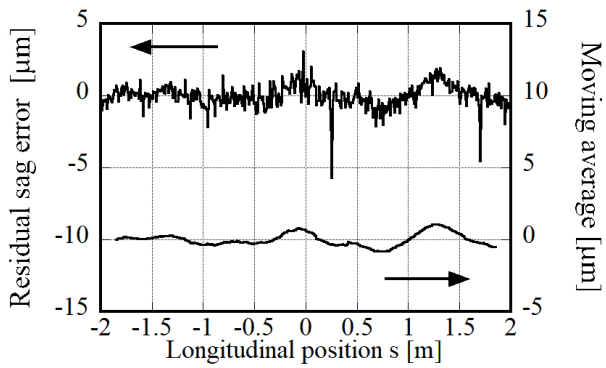

Figure 2: Example of residual sag error distribution in the longitudinal direction with two kinks.

To evaluate the overall random error of the vibrating-wire alignment technique, we repeatedly measured the displacements of *Q05* and *SD1* 20 times on the common girder *B* without adjusting the positions of the magnets. We removed the wire once, and then reinstalled the same wire or new wire between the measurements. We redefined the reference line after each measurement. The peak-to-peak value of the changes in the displacement was less than ±3 µm.

We demonstrated precise alignment on the common girder *B*. The displacements of *SD1*, *SF1*, *Q05*, *SF2* and *SD2* were suppressed to less than 8 µm. To simulate the transport to the tunnel, we moved the girder *C* to other experimental room. Changes in the displacement by the transport test are listed in Table 2. Because the changes exceeded the above overall random error, changes in the magnet positions on the girder, or a deformation of the girder during and after the transport was not negligible.

Wire Alignment Monitoring System

After the installation of vacuum chamber, a wire cannot be installed at the center of the bore. To measure a long-term drift of the magnet position, we developed an additional instrument, a Wire Alignment Monitoring System (WAMS) [10]. A wire is tensioned above the multipole magnets. The wire is fixed on the both ends magnets of the common girder.

Table 2: Changes in the Displacement by the Transport Test

Magnet name	VW Technique (x, y) [µm]	WAMS (x, y) [µm]
Q08	(+8, -3)	(+11, +2)
Q09	(+7, +4)	(+8, +7)
SX0	(-3, -3)	(+3, +3)

We placed sensors of the WPS on the reference points of the other magnets. By measuring the wire position, change in the magnet position can be evaluated.

Since we also plan to measure the change in the magnet position due to the transport using the WAMS, in the transport test of the girder *C* described above, changes in the magnet positions were measured (see Table 2). Maximum difference between the measurements by the WAMS and the VW technique was 6 µm. So we conclude that the WAMS has sufficient precision to monitor the relative changes of magnet positions in our alignment procedure.

SUMMARY

We have developed prototype magnets and common girders for SPring-8-II, and integrated the test half-cell. We demonstrated our precise magnet alignment procedure on the common girder, and evaluated the error budget. We found a deterioration of the alignment accuracy caused by the girder transport after the alignment. We plan to repeat the transport tests to figure out the cause of the change.

ACKNOWLEDGEMENTS

The authors are grateful to H. Tanaka and T. Ishikawa for support throughout the development of our magnet system. This work was supported by the RIKEN SPring-8 Center (RSC) and by JSPS KAKENHI Grant Number 2639123.

REFERENCES

[1] H. Tanaka *et al.*, Proc. of IPAC2016, Busan, Korea, 2016, pp. 2867-2870.

[2] T. Watanabe *et al.*, Physical Review Accelerator and Beams, 20, 072401 (2017).

[3] T. Watanabe *et al.*, Proc. of IPAC2014, Dresden, Germany, 2014, pp. 1253-1255.

[4] G. Le Bec *et al.*, Physical Review Special Topics Accelerator and Beams, 15, 022401 (2012).

[5] T. Aoki *et al.*, Proc. of the 15 th Annual Meeting of Particle Accel-erator Society of Japan, Nagaoka, Japan, 2018.

[6] A. Jain *et al.*, Proc. of IWAA2008, Tsukuba, Japan, 2008, pp. 1-6.

[7] C. Yu *et al.*, Proc. of IWAA2012, Batavia, U.S.A., 2012.

[8] L. Tsai *et al.*, Proc. of PAC2007, New Mexico, U.S.A., 2007, pp. 395-397.

[9] K. Fukami *et al.*, Review of Scientific Instruments, 90, 054703 (2019).

[10] C. Zhang *et al.*, Proc. of IWAA2016, Grenoble, France, 2016.